Dual-Gas Quartz-Enhanced Photoacoustic Sensor for Simultaneous Detection of Methane/Nitrous Oxide and Water Vapor

Dual-gas quartz-enhanced photoacoustic sensor for simultaneous detection of methane/nitrous oxide and water vapor

Arianna Elefante,[†,‡] Marilena Giglio,[†,‡] Angelo Sampaolo,[†,‡] Giansergio Menduni,[‡§] Pietro Patimisco,[†,‡] Vittorio M. N. Passaro,[§] Hongpeng Wu,[†] Hubert Rossmadl,[‖] Verena Mackowiak,[‖] Alex Cable,[⁋] Frank K. Tittel,[δ] Lei Dong,[*†] and Vincenzo Spagnolo[*†,‡]

[†] State Key Laboratory of Quantum Optics and Quantum Optics Devices, Institute of Laser Spectroscopy, Shanxi University, Taiyuan 030006, China

[‡] PolySense Lab – Dipartimento Interateneo di Fisica, University and Politecnico of Bari, Via Amendola 173, Bari, Italy

[§] Photonics Research Group, Dipartimento di Ingegneria Elettrica e dell'informazione, Politecnico di Bari, Via Orabona 4, Bari, 70126, Italy;

[‖] Thorlabs GmbH, Hans-Boeckler-Straße 6, 85221 Dachau, Germany

[⁋]Thorlabs, Inc., 56 Sparta Ave., Newton, 07860, USA

[δ]Department of Electrical and Computer Engineering, Rice University, Houston, Texas 77005, USA

ABSTRACT: The development of a dual-gas quartz-enhanced photoacoustic (QEPAS) sensor capable of simultaneous detection of water vapor and alternatively methane or nitrous oxide is reported. A diode laser and a quantum cascade laser (QCL) excited independently and simultaneously both the fundamental and the first overtone flexural mode of the quartz tuning fork (QTF), respectively. The diode laser targeted a water absorption line located at 7181.16 cm^{-1} (1.392 μm), while the QCL emission wavelength is centered at 7.71 μm and was tuned to target two strong absorption lines of methane and nitrous oxide, located at 1297.47 cm^{-1} and 1297.05 cm^{-1}, respectively. Two sets of micro-resonator tubes were positioned, respectively, at the antinode points of the fundamental and the first overtone flexural modes of the QTF to enhance the QEPAS signal-to-noise ratio. Detection limits of 18 ppb for methane, 5 ppb for nitrous oxide and 20 ppm for water vapor have been achieved at a lock-in integration time of 100 ms.

Gas spectroscopic techniques based on optical absorption have been widely demonstrated as fast, highly sensitive and selective tools to detect and monitor one or more gas species in a mixture.[1,2] Once a low-noise, narrow-bandwidth laser source and a strong, interference-free absorption line are selected, several sensing approaches can be employed.[1] Multi-pass cells allow an increase of the optical pathlength up to one order of magnitude.[3] High-finesse optical cavities exploit optical field enhancement when operating in a steady-state regime, allowing an increase of the intra-cavity optical power by more than two orders of magnitude.[4] Both approaches require fast, low-noise, ultra-sensitive optical detectors to acquire the weak optical field exiting the multi-pass cell or the cavity. Moreover, these techniques suffer from mechanical instability and complex optical alignment procedures and are strongly wavelength-dependent, hence limiting their optical coupling with multiple sources. Photoacoustic (PAS) spectroscopy is also based on an optical absorption process but differs in the way the absorption signal is detected. In PAS sensors, the gas is confined inside an acoustic cell and the exciting laser light is modulated at one of the cell acoustic resonance frequencies. The modulated absorption and non-radiative relaxation occurring in the gas generate pressure waves, i.e. sound. These waves are then detected by using low-noise, highly-sensitive microphones.[5] Quartz-enhanced photoacoustic spectroscopy (QEPAS) exploits an alternative sound detection approach, by substituting the resonant cell and microphone with a quartz tuning fork (QTF), acting as a sharply resonant acoustic transducer.[2] The QTF can be coupled with a pair of micro-resonator tubes in order to confine and amplify the sound waves. In on-beam QEPAS, micro-resonator tubes are aligned on both sides of the QTF, close to one of the antinode points of a QTF in-plane flexural resonance mode.[6] The laser beam is focused through the tubes and between the prongs and is modulated at the resonance frequency (or one of its subharmonics) of the selected QTF vibrational mode. The pressure wave deflects the prongs and an electrical signal proportional to the stress field is generated exploiting the quartz piezoelectricity. QEPAS sensors can be very compact, do not require an optical detector and are wavelength independent. Indeed, the QTF response depends only on the sound waves intensity and not on the wavelength of the exciting laser used, which makes it suitable for coupling multiple sources emitting at different wavelengths for multi gas detection. Many gas sensing applications require simultaneous detection and quantification of different components in a gas mixture, such as detection of isotopes

concentration ratio, environmental monitoring of greenhouse gases, monitoring of different biomarkers in human breath[7] and study of molecular relaxation dynamics.[8] Different approaches have been explored to achieve multi-gas detection. One possibility is to exploit a single laser source with a wavelength tuning range covering absorption lines of the different gas targets.[9,10] Optically coupling an external cavity with Fabry-Perot quantum cascade lasers (QCLs), a tunability range of more than 100 cm^{-1} can be achieved. The QCLs emission wavelength can be finely tuned by a rotating grating to target different gas species.[11] However, external cavity QCLs are bulky, suffering from power fluctuations and the emission wavelength stability is limited by mechanical instability of the grating. Another approach to widely tune a QCL is to integrate a heater to the laser chip. A QCL with an integrated-heater operating in the 1276-1284 cm^{-1} region was implemented to detect methane and acetylene for combustion applications.[9] Although the high time resolution achieved (20-40 μs), this approach can be applied only to the case in which the absorption lines of the different gases are separated by few cm^{-1}. An alternative approach employs multiple laser sources, one for each gas to be detected, switching between them and activating one laser at one time. A photoacoustic sensor was developed with five lasers sequentially operated along a single optical interaction path using a scanning galvanometer as an optical multiplexer with the capability of switching between two lasers in less than 1 s.[12] QEPAS is perfectly suitable for multi-gas sensing applications requiring either a wide tuning range of the exciting laser source or the employment of multiple sources[14] due to the wavelength independence responsivity of the QTF. In Ref. [14], a single intercascade laser was tuned to target absorption features of methane, ethane and propane, while in Ref. [15] the emission wavelength of a distributed feedback-QCL (DFB-QCL) was tuned to detect carbon monoxide and nitrous oxide. In Ref. [16] two lasers matching the absorption lines of methane and ammonia, respectively, were alternatively focused through the QEPAS detection module.

In all the cases reviewed so far there is a finite time interval between the detection of several gas species, which corresponds to the time needed to tune the laser emission wavelength between different absorption features and/or to switch between multiple laser sources. Hence, these approaches can be referred to as quasi-simultaneous dual-gas detection. Differently, in Ref**.** [17] a photoacoustic sensor was developed with three lasers in combination with three independent resonators along three optical paths. Sub part-per-million detection limits for CH_4, H_2O and HCl were demonstrated, but the cross-talking among the resonators did not allow a real-simultaneous detection of the gases. A multi-gas QEPAS sensor based on three bare QTFs with different response frequencies for trace gas detection was reported in Ref. [18]. Three near-infrared laser diodes were used to simultaneously monitor water vapor, methane and acetylene in the parts per million range.

A straightforward way to guarantee simultaneous detection is developing a wavelength-modulation division multiplexing (WMDM) scheme.[19] Different laser sources are independently modulated, one for each gas species to be detected and then combined using a single detector. The recorded signal is then demodulated at the different modulation frequencies. Optical sensors with WMDM configuration based on multi-pass absorption have been reported in the literature.[20,21] The development of custom QTFs opened the way to exploit QEPAS technique in WMDM configuration.[22] If the QTF frequency of the in-plane flexural mode is decreased to a few kHz, the frequency of the in-plane first overtone mode, which is ~ 6.2 times higher than the fundamental one, becomes accessible for QEPAS operation. A proof-of-concept of simultaneous dual-gas QEPAS detection exploiting a custom QTF was reported in Ref. [23], where two DFB diode lasers operating in the near-IR region were used as the excitation sources for the fundamental and the first overtone mode of a bare QTF and simultaneous detection of water vapor and acetylene was demonstrated.

In this work, a WMDM configuration dual-gas QEPAS sensor operating in two different spectral regions, near-IR and mid-IR, is reported. A DFB-QCL emitting at 7.7 μm allowed methane (CH_4) or nitrous oxide (N_2O) detection, while a diode laser emitting at 1.392 μm was exploited for simultaneous water vapor monitoring. In contrast to the approach proposed in Ref. [18], which precludes the use of a micro-resonator system, the dual gas QEPAS sensor presented here employed a custom QTF acoustically coupled with two micro-resonator dual-tube systems to enhance both the fundamental and the first overtone QEPAS signal-to-noise ratio, thereby lowering the detection limits down to concentrations in the part per billion range.

EXPERIMENTAL SECTION

Dual-gas spectrophone design. Simultaneous dual-gas detection with QEPAS technique can be obtained only by exciting at the same time two different flexural vibrational modes of a QTF, i.e. the fundamental and the first overtone mode. The related resonance frequencies can be chosen at the design phase by properly selecting the prongs length and thickness and making both modes suitable for QEPAS operation. In Ref. [24], three different QTF designs were proposed and tested, having both the fundamental and the first overtone mode frequencies lower than 40 kHz. Among them, we selected the QTF labelled as QTF#1 since it showed the highest quality factor value and consequently the best QEPAS performance, for both modes. QTF#1 has two rectangular prongs with length of 17 mm, thickness of 1 mm and a quartz crystal width of 0.25 mm. These QTF geometrical parameters leads to a fundamental frequency as low as 2.88 kHz, while the first overtone mode resonates at ~17.78 kHz. The spacing between the two prongs is 0.7 mm. The fundamental mode has an antinode point on the top of the QTF while the first overtone mode has two antinode points, one coincident to that of the fundamental mode and the other one close to the middle of the prong (at 9 mm from the QTF#1 top). In this work, two pairs of micro-resonator tubes were employed to simultaneously enhance the fundamental and the overtone mode. One pair was located at 2 mm from the top of the prongs for the fundamental mode and the other pair at 9.5 mm from the top of the prongs for the first overtone mode, as discussed in Ref. [24]. The length and internal diameter of tubes must be accurately selected to optimize the QEPAS performance of the spectrophone.[25] The length of the tubes is correlated to the sound

wavelength by the relation $\lambda_s = v/f$, where v is the sound speed and f is the QTF resonance frequency.[26] The optimal tube length was experimentally found to be between $\lambda_s/4$ and $\lambda_s/2$. For the first overtone mode, the corresponding length range is 4.8 mm < l < 9.6 mm, and l = 8.5 mm was selected. For the fundamental mode, the optimal length falls between 30 mm and 60 mm. However, such a length would require a bulky acoustic detection module to accommodate the spectrophone and thus complicate the optical alignment operations. For these reasons, tubes with a length of 9.5 mm have been employed, which are 1 mm longer than the tubes used for the first overtone mode in order to maintain the spectrophone size as compact as possible. A low QEPAS signal enhancement is thus expected for the fundamental mode. Therefore, this mode was chosen to detect the gas target with the highest concentration. For both antinodes, tubes having an ID=1.36 mm were mounted, which was proved to be the optimum internal diameter in terms of the signal-to-noise enhancement factor with respect to the bare QTF. The gap between tubes and the QTF surface was set to 150 μm. A schematic of the spectrophone is shown in Fig. 1.

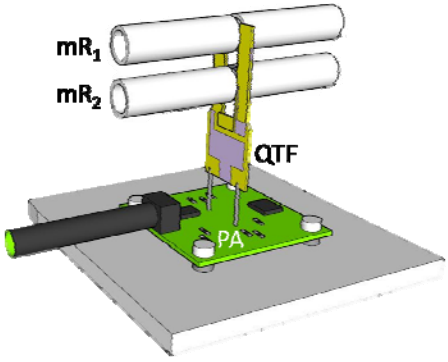

Figure 1. Schematic of the spectrophone implemented. The QTF is coupled with two pairs of micro-resonators tubes aligned perpendicularly to the QTF. The first pair of tubes (mR_1), each one 9.5 mm long, is located at the fundamental antinode point near the QTF top, the second pair (mR_2), each tube 8.5 mm long, is positioned 9.5 mm below the prongs top, at the second antinode point position of the QTF first overtone mode; the pre-amplifier (PA) board is shown on the bottom.

The vibrational properties of the QTF coupled with the micro-resonator tubes, namely the resonance frequency and the quality factor of both flexural modes were measured by electrically exciting the QTF. A sinusoidal voltage signal excites the QTF resulting in a piezoelectric charge displacement on its prongs via an inverse piezoelectric effect. Charges are collected by electrodes deposited on the QTF surface and the QTF current signal is converted into an output voltage by means of a trans-impedance preamplifier. Finally, the output voltage is demodulated by a lock-in amplifier at the same frequency of the excitation signal. The resonance curves for the fundamental and first overtone mode of a bare QTF were fitted using a Lorentzian function to extract the resonance frequencies and the full width at half maximum (FWHM) values. The quality factor is calculated as Q = f/FWHM. In Fig.2, the QTF resonance curves of the fundamental and first overtone modes measured at 200 Torr are shown. The fundamental mode exhibits a resonance frequency of f_0 = 2871.05 Hz and a quality factor of 6680, while the overtone resonance mode occurs at f_1 = 17747.70 Hz with a quality factor of 17070.

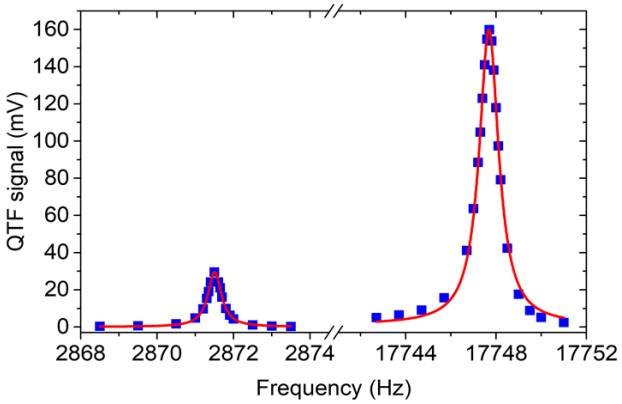

Figure 2. Spectrophone resonance curves (blue squares) and related Lorentzian fits (red solid curves) of the fundamental and the first overtone modes at 200 Torr in air.

The first overtone mode exhibits a higher quality factor with respect to the fundamental one as already demonstrated in Ref. [24]. The fundamental mode will be used to monitor the water vapor concentration in air (whose concentration is expected to be in the percent-range), while the first overtone mode will be exploited to detect CH_4 and N_2O trace gas concentration. The distance between the fundamental antinode point and the second antinode of the first overtone mode is ~ 8 mm, allowing an easy alignment of the two laser beams through the micro-resonator tubes.

Architecture of dual-gas QEPAS sensor. The dual-gas spectrophone is enclosed in a gas cell, forming the acoustic detection module (ADM). The gas cell is equipped with a ZnSe window anti-reflection (AR)-coated in the range of 7-12 μm on the front side and a N-BK7 window AR-coated in the 1-1.7 μm range on the back side. Two connectors are used as a gas inlet and a gas outlet. The ADM was implemented in the QEPAS sensor setup depicted in Fig. 3. Two lasers were used as excitation sources. A DFB-QCL emitting at 7.73 μm was used to alternately target methane and nitrous oxide absorption peaks exciting the first overtone QTF mode. The beam was then focused through the microresonator tubes located at the lower antinode point of the overtone mode by means of a 7-12 μm AR-coated Zn-Se lens having a focal length of 75 mm. A pinhole was used as a spatial filter to cut the laser beam tails and prevent that the incident light hits the QTF prongs or the micro-resonator tubes and generates a background photothermal noise. A diode laser emitting at 1.392 μm was used to target water vapor. A 1.05 – 1.7 μm AR-coated N-BK7 lens having a focal length of 75 mm was used to focus the diode laser beam between the QTF prongs and through the tubes located at to the antinode point of the fundamental mode. The beam waists of the QCL and the diode laser measured on the QTF plane have a diameter of 0.28 mm and 0.24 mm, respectively, well below the prong spacing of the QTF (0.7 mm). The portion of optical power transmitted through the micro-resonator tubes and between the prongs was 97.5% and 99.2% for the

QCL and the diode laser, respectively. QEPAS signals were detected using the wavelength modulation technique with 2*f*-detection and the two lasers were independently modulated.

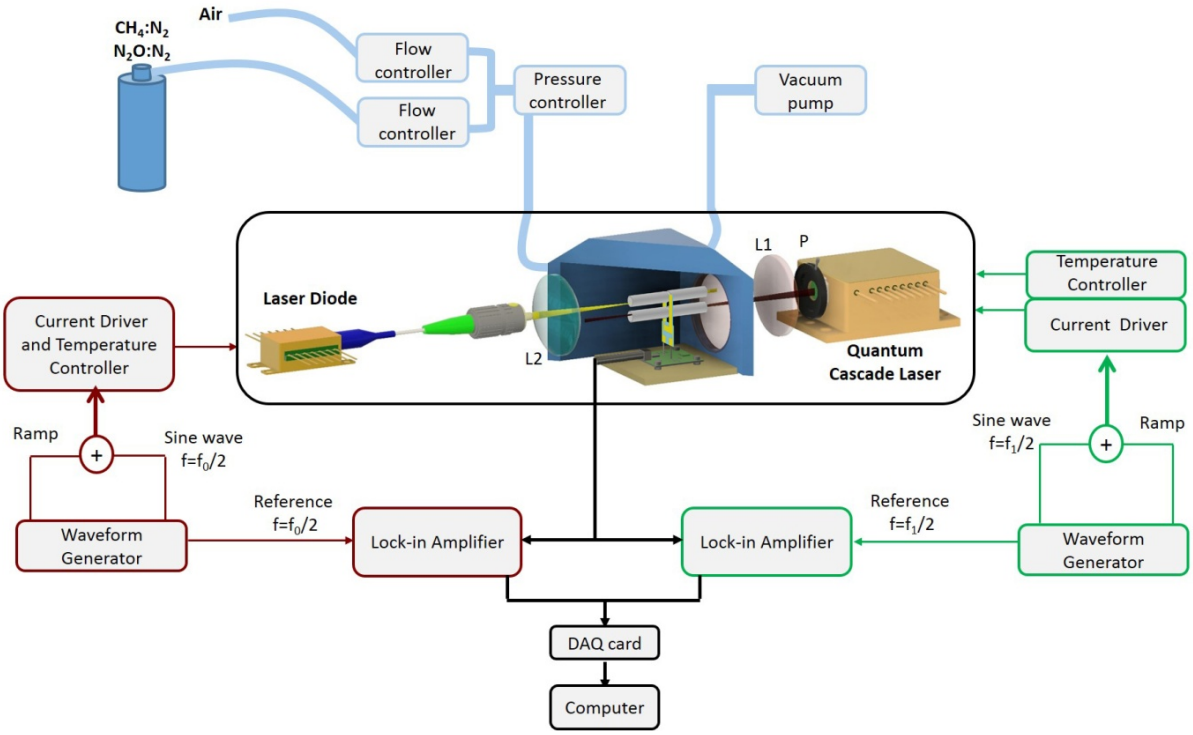

Figure 3. Schematic of the dual-gas QEPAS sensor. P - Pinhole; L1 - AR-coated Zn-Se lens; L2 - AR-coated N-BK7 lens; DAQ – Data Acquisition Board.

A sinusoidal dither was applied to the current driving the diode laser at the half of the fundamental mode frequency $f_0/2$ = 1435.52 Hz, while the current injected into the QCL was modulated at the half of the first overtone mode frequency, $f_1/2$ = 8873.85 Hz. The QTF signal was converted into a voltage signal using a trans-impedance preamplifier with a gain factor of 30; and then was simultaneously demodulated at the fundamental and first overtone frequencies using two lock-in amplifiers. The integration time was set at 100 ms for both lock-in amplifiers. The demodulated signals were recorded and analyzed on a personal computer by using a multi-channel data acquisition card from National Instruments. A gas line system was assembled to manage flow rates, pressures and compositions of the gas mixtures to be analyzed. One Y-ended gas line branch was connected to the gas cylinders containing certified concentrations of gas targets: 10000 ppm of CH_4 in N_2 and 10000 ppm of N_2O in N_2. The other gas line branch was connected to a valve allowing laboratory air to enter the line. Since the water vapor concentration in the laboratory environment can vary, a Nafion humidifier was inserted just before the ADM (not shown in Fig. 3) to keep the water concentration in the ADM fixed to 1.6%. The pressure inside the ADM was fixed at 200 Torr and the flow set at 25 sccm by means of a pressure controller, a valve system and a vacuum diaphragm pump.

RESULTS AND DISCUSSION

Simultaneous QEPAS detection of methane and water. As a first step, the QEPAS sensor was tested for detection of methane and water vapor in a gas mixture, independently. The QCL and diode laser were alternatively switched on to excite the targeted CH_4 and H_2O absorption lines, respectively. A preliminary study showed that the CH_4 QEPAS signal is maximized at a gas pressure of 200 Torr. The HITRAN database[27] was used to simulate the absorption cross-section of pure methane at 200 Torr in the QCL tunability range from 1298 cm^{-1} to 1297.4 cm^{-1}. The simulation result is depicted in Fig. 4(a). The strongest absorption peak of methane falls at 1297.47 cm^{-1} with a linestrength of $3.9 \cdot 10^{-20}$ cm/molecule. No visible water lines fall in the investigated QCL emission spectral range. Figure 4(b) shows the corresponding QEPAS spectral scan acquired for a mixture of 1000 ppm of CH_4 with 1.6% of water vapor at 200 Torr. The QCL temperature was set to 12.5 °C and the injected current was scanned in the range 207-257 mA applying a 2 mHz ramp to the current driver. The QEPAS signal was demodulated at f_1 for methane detection. The amplitude of the QEPAS signal related to the selected line (targeted at a laser current of I_{QCL}= 243.7 mA) was optimized by varying the laser modulation depth. The highest CH_4 signal of 146 mV was observed at a modulation depth of 35 mV. The other features composing the QEPAS spectrum of Fig. 4(b), like the ones peaked at 224.8 mA and 231.8 mA, correspond to methane absorption lines with weaker linestrenghts as confirmed by a HITRAN database simulation. The QCL was then turned off and the diode laser was used to excite the water vapor ab-

sorption line. Figure 4(c) shows the simulated absorption cross-section of pure water at 200 Torr in the 7180-7185 cm^{-1} range, obtained using the HITRAN database.[27] Within the current dynamic range of the diode, the strongest absorption peak of H_2O falls at 7181.16 cm^{-1} with a linestrength of $1.4 \cdot 10^{-20}$ cm/molecule. Figure 4(d) shows the QEPAS spectral scan for a mixture of 1000 ppm of CH_4 with 1.6 % of water vapor, at 200 Torr.

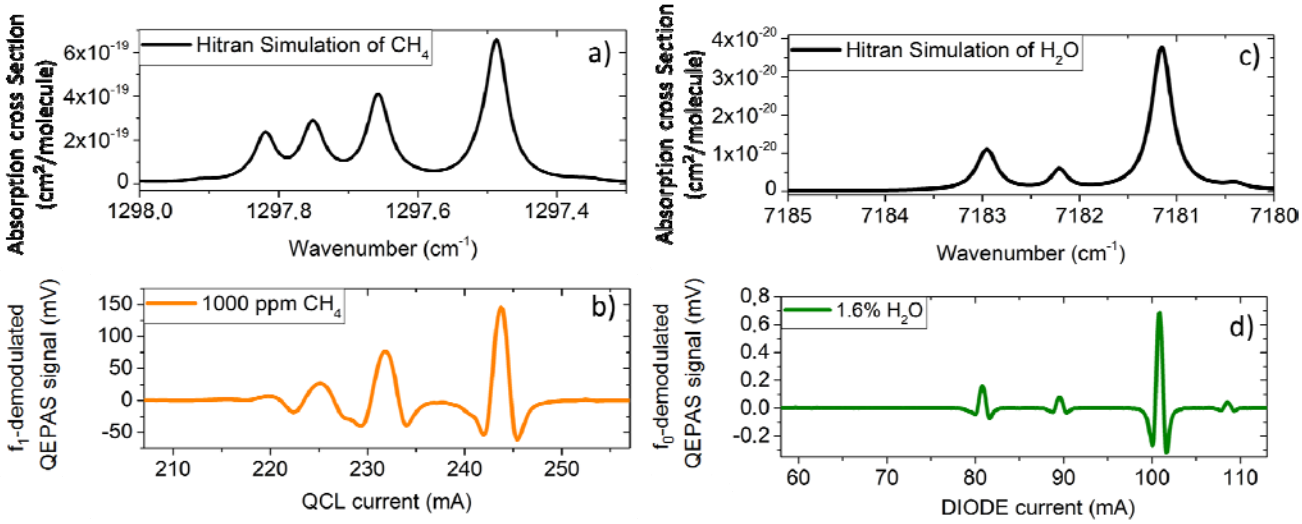

Figure 4 (a) Hitran simulation of the pure methane absorption cross-section at 200 Torr; (b) QEPAS spectral scan of 1000 ppm of CH_4 at 200 Torr measured by demodulating the QTF signal at the overtone mode frequency; c) Hitran simulation of the pure water vapor absorption cross-section at 200 Torr; d) QEPAS spectral scan of 1.6% of H_2O at 200 Torr measured by demodulating the QTF signal at the fundamental mode frequency.

These measurements were obtained by setting the temperature of the laser diode to 25 °C and scanning the laser current in the range 50-115 mA, by applying a 2 mHz ramp to the current driver. The diode modulation amplitude was set to 12 mV and the QEPAS signal was demodulated at f_0. The selected H_2O line shows a peak value of 0.68 mV. The QEPAS absorption features at 80.7 mA, 89.5 mA and 108.6 mA correspond to water vapor absorption lines with weaker linestrenghts. The optical power focused inside the ADM was 128.0 mW at the QCL current set to target the selected CH_4 absorption line and 6.2 mW for the diode laser current set to hit the strongest H_2O line absorption line.

It is mandatory to verify that the QEPAS signal demodulated at f_0 is not influenced by the first overtone mode vibration and that the QEPAS signal demodulated at f_1 is not affected by the fundamental mode vibration. Therefore, a preliminary test was conducted to investigate the QTF response while simultaneously exciting the fundamental and first overtone vibrational modes. Figure 5(a) shows the QTF signal demodulated at f_1 when the QCL excites the first overtone mode of the QTF (orange squares) and when both the QTF vibrational modes are simultaneously excited by the two laser sources (blue circles).

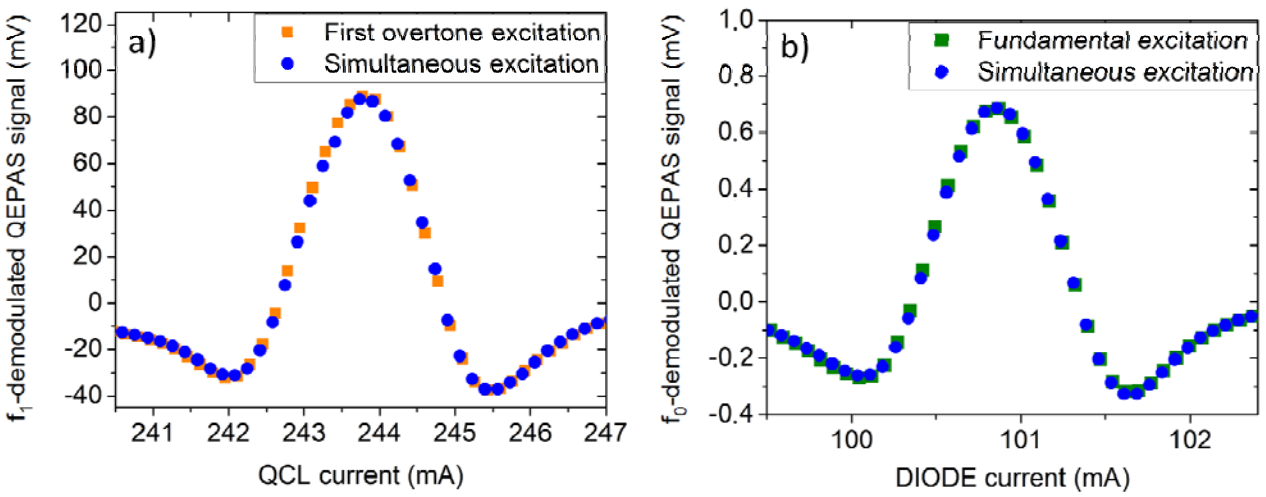

Figure 5. (a) QEPAS spectral scan of the methane absorption line at 1297.47 cm^{-1} detected at the first overtone mode when only the first overtone mode is excited (orange squares) or both the fundamental and the first overtone modes are excited (blue circles). (b) QEPAS spectral scan of the water vapour absorption line at 7181.16 cm^{-1} detected at the fundamental mode when only the fundamental mode is excited (green squares) or both the fundamental and first overtone modes are excited (blue circles).

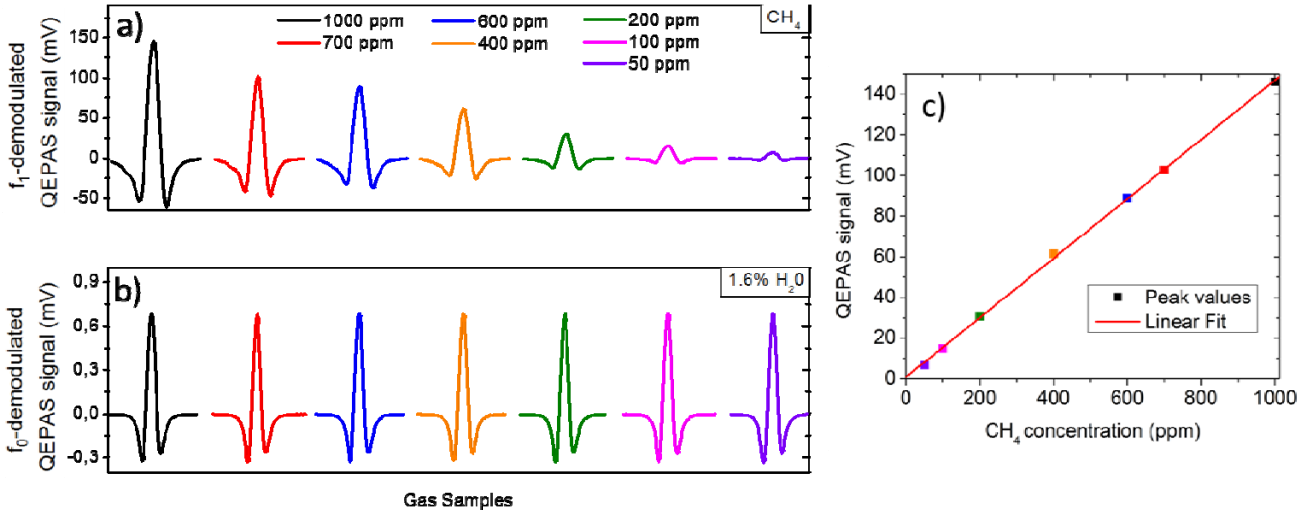

Figure 6. (a) Spectral scans of the methane absorption line at 1297.47 cm^{-1} for different CH_4 concentrations in humidified air with 1.6% water vapor. (b) Corresponding spectral scans of the water absorption line at 7181.16 cm^{-1} for CH_4 each dilution, confirming that the H_2O concentration was kept constant. Simultaneous spectral scans are represented by the same curve color. (c) Peak values for each CH_4 concentration (square symbols) and the corresponding best linear fit (red line).

The QCL and the diode laser currents were tuned to detect the selected CH_4 and H_2O absorption lines falling at 1297.47 cm^{-1} and 7181.16 cm^{-1}, respectively, in a mixture containing 600 ppm of CH_4 and 1.6% of water vapor. Similarly, Fig. 5(b) shows the QTF signal demodulated at f_0 when only the fundamental vibrational mode is excited using the diode laser (green squares) and when both the lasers operate (blue circles). The perfect overlap between the curves in both figures indicates that there is no cross-talking between the QTF fundamental mode and first overtone mode operations, even in the presence of the two micro-resonator tubes placed at the antinode points. This allows the excitation of the two vibrational modes simultaneously, acquisition of the QTF signal and independent demodulation at the two resonance frequencies to identify the contribution due to each gas species and retrieve both gas concentrations. The calibration of the sensor for methane detection was performed acquiring spectral scans of mixtures of CH_4 in laboratory air with different gas target concentrations, ranging from 50 to 1000 ppm. In all generated mixtures, the water vapor concentration was fixed to 1.6% by using the Nafion humidifier. The sensor was used in the dual-gas detection mode in order to measure the CH_4 concentration and sim-

ultaneously monitor the water vapor level. Figure 6(a) shows the QEPAS signal acquired for methane at seven different concentrations and the correlated water QEPAS signal (see Fig. 6(b)).

The CH_4 peak values were extracted for each spectral scan and plotted as a function of the concentration in Fig. 6(c). A linear fit of the experimental data points was performed to obtain the sensor calibration curve for methane. The squared-R value of 0.999 confirms the linearity of the QEPAS signal with the methane concentration, with a slope of 0.146 mV/ppm and an intercept of 0.85 mV. For each dilution, the water vapor level has been monitored by scanning the H_2O absorption line with the diode laser. The H_2O QEPAS peak signals extracted from Fig. 6(b) show a peak value fluctuation < 0.25% value, demonstrating the capability of the Nafion humidifier to efficiently fix the water concentration in the gas line. For CH_4, a 1σ-noise level of 2.7 μV was estimated at 100 ms lock-in integration time corresponding to a minimum detection limit (MDL) of 18 part-per-billion (ppb), while for H_2O with a 100 ms integration time we obtained a 1σ noise of 1.0 μV corresponding to an MDL of 20 ppm.

Simultaneous QEPAS detection of nitrous oxide and water. The realized QEPAS sensor allows also the simultaneous detection of water vapor and nitrous oxide, since the QCL emission spectral range covers absorption lines of N_2O. With the QCL temperature set to 12.5 °C and the QCL current scanned in the range of 152-287 mA, several N_2O absorption lines can be targeted. The highest intensity line falls at 1297.05 cm^{-1} with a linestrength of $1.7 \cdot 10^{-19}$ cm/molecule. The QCL modulation amplitude and the gas pressure maximizing the N_2O QEPAS signal were found to be 130 mV and 200 Torr, respectively. For water vapor detection, the diode laser working conditions remain the same as before. Figure 7(a) shows the QTF signal demodulated at f_1 for a mixture of 400 ppm N_2O and 1.6% H_2O in air. The selected N_2O absorption line is excited at a QCL current of I_{QCL}=271.1 mA and shows a peak value of V= 227 mV. The sensor was calibrated for N_2O detection in the range of 300-800 ppm starting from a 10000-ppm certified concentration of N_2O:N_2. The QEPAS peak value scales linearly with N_2O concentration in the selected range with a slope of 0.60 mV/ppm, an intercept of 0.51 mV and a squared-R value of 0.997, as shown in Figure 7(b). A 1σ-noise level of 2.7 μV at an integration time of 100 ms corresponds to an MDL of 5 ppb for N_2O detection. Furthermore, an analysis of the stability of the dual-gas sensor was performed by acquiring the QEPAS signal of N_2O and H_2O vapor for 20 minutes. This analysis is usually performed by fixing the laser current to correspond to the gas absorption peak, while the gas keeps flowing in the gas line. To avoid QEPAS signal fluctuations due to the possible laser sources instabilities and drifts, we applied two fast voltage ramps to the QCL and diode laser in order to scan the selected N_2O and H_2O absorption lines, respectively. The results are shown in Fig. 8. The peak-to peak amplitude V_{ramp} and frequency f_{ramp} of the ramps applied to the diode laser and to the QCL were 15 mV and 30mHz, and 60 mV and 50 mHz, respectively. The f_{ramp} values were selected to provide a fast absorption line scan and avoid down-sampling reconstruction.

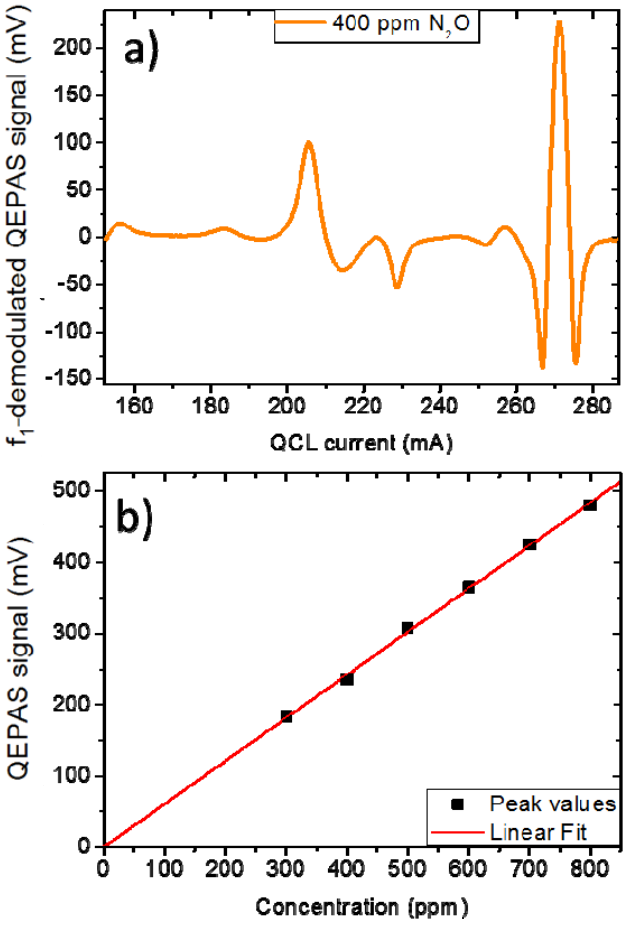

Figure 7. (a) Nitrous oxide spectral scan detected at f_1 exciting the first overtone vibrational mode of the QTF with the quantum cascade laser for a mixture of 400 ppm of nitrous oxide and 1.6% of water in air at 200 Torr. (b) Peak values for each N_2O concentration (square symbols) and the corresponding best linear fit (red line).

As clearly visible in Fig. 8, both the H_2O and N_2O peak signal values remain nearly constant with fluctuations lower than 0.9%, demonstrating the time stability of the dual gas QEPAS sensor.

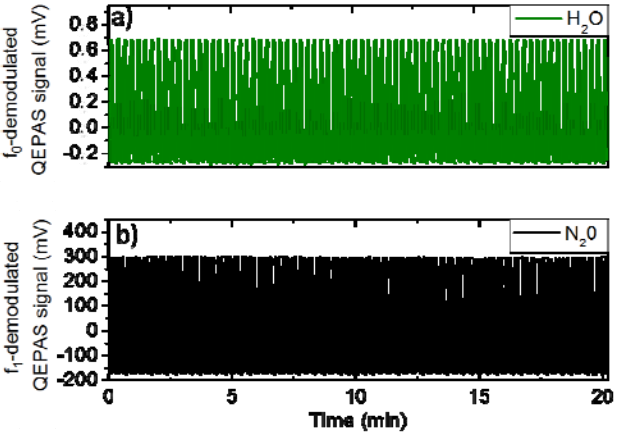

Figure 8. Simultaneous QEPAS spectral scans for a mixture of 600 ppm of nitrous oxide in humidified air (a) H_2O vapor signal detected at f_0 applying a narrow ramp to the diode laser current centered on the water vapor line at 7181.16 cm^{-1}. (b) N_2O signal detected at f_1 applying a narrow ramp to the QCL current centered on the N_2O absorption line at 1297.05 cm^{-1}.

CONCLUSIONS

In this work we reported on the realization of a dual-gas QEPAS system operating in the near- and mid-IR, capable of simultaneous detection of two different gas species in a mixture. The sensor was based on a frequency-modulated multiplexing scheme. A custom QTF allowed the simultaneous excitation of the fundamental and the first overtone flexural modes using a near-IR diode laser and a mid-IR DFB-QCL as excitation sources. The feasibility of the simultaneous detection of water vapor/methane and water vapor/nitrous oxide was demonstrated. The sensor was calibrated for the detection of methane and nitrous oxide with a constant concentration of water vapor fixed at 1.6%, showing a linear response of the QEPAS signals with the gas target concentration. The minimum detection limits achieved were 18 ppb for CH_4, 5 ppb for N_2O and 20 ppm for water vapor, at a lock-in integration time of 100 ms. The developed QEPAS sensor is suitable for real-time simultaneous detection of two gas species in ambient air, and in particular to detect one gas species (methane or nitrous oxide) and monitor the water vapor in the mixture. This is particularly important for QEPAS sensing, since when operated with slow relaxing gas, such as NO, CO or CO_2, and CH_4 water vapor acts as promoter of the vibrational-translation (V-T) energy relaxation processes. The methodology proposed in this work is based on the use of a Nafion humidifier combined with a gas mixture flow rate of 25 sccm. With such a small flow, the Nafion humidifier is able to provide a constant concentration of water vapor, which is a mandatory condition to guarantee reliable concentration measurements for methane. An alternative approach can be based on a full characterization of the methane photoacoustic response with respect to water vapor concentration from the ppm range up to the standard atmospheric concentration level. Once the correlation between the methane signal enhancement and the water vapor partial pressure is retrieved, a QEPAS dual gas sensor with a similar setup can be implemented to perform an instantaneous self-calibration of the sensor. This can be crucial for applications like environmental monitoring or breath sensing, where large variations of water vapor concentration can occur.

AUTHOR INFORMATION

Corresponding Authors

* E-mails v.spagnolo@poliba.it; donglei@sxu.edu.cn

Author Contributions

The manuscript was written through contributions of all authors. All authors have given approval to the final version of the manuscript.

Notes

The authors declare no competing financial interest.

ACKNOWLEDGMENTS

Financial support from THORLABS GmbH, within the joint-research laboratory PolySense is acknowledged. Lei Dong acknowledges support by National Natural Science Foundation of China (Grants #61622503, 61575113). Frank K. Tittel acknowledges support by the National Science Foundation (NSF) ERC MIRTHE, NSF NeTS R3H685 and the Robert Welch Foundation (C0586).

REFERENCES

(1) Hodgkinson, J.; Tatam, R.P. *Meas. Sci. Technol.* **2013**, *24*, 012004.
(2) Patimisco, P.; Sampaolo, A.; Dong, L.; Tittel, F. K.; Spagnolo, V. *Appl. Phys. Rev.* **2018**, *5(1),* 011106.
(3) Werle, P.; Slemr, F.; Maurer, K.; Kormann, R.; Mucke, R.; Janker, B. *Opt. Laser Eng.* **2002**, *37*, 101–114.
(4) Gagliardi, G.; Loock, H.P. Cavity-enhanced spectroscopy and sensing. *Springer,* Berlin, Heidelberg, **2014**.
(5) Sigrist, M.W. *Air Monitoring by Spectroscopic Techniques*, Wiley: New York, NY, USA, 1994.
(6) Dong, L.; Kosterev, A.A; Thomazy, D.; Tittel, F.K. *Appl. Phys. B* **2010**, *100*, 627–635.
(7) Fortes, P.R.; Petruci, J.F.S.; Raimundo, I.M. Optical Gas Sensors for Exhaled Breath Analysis. *SPIE Press*, Bellingham, Washington, 98227-0010 USA, **2017**.
(8) Wysocki, G.; Kosterev, A.A.; Tittel, F.K *Appl. Phys. B* **2006**, *85*, 301-306.
(9) Zhang, G.; Khabibullin, K.; Farooq, A. *Proc Combust Inst.* **2019**, *37.2*, 1445-1452.
(10) Cao, Y.; Sanchez, N.P.; Jiang, W.; Griffin, R.J.; Xie, F.; Hughes, L.C.; Zah, C.; Tittel, F.K. *Opt. Express* **2015**, *23.3*, 2121-2132.
(11) Hugi, A.; Terazzi, R.; Bonetti, Y.; Wittmann, A.; Fischer, M.; Beck, M.; Faist, J.; Gini, E. *Appl. Phys. Lett.* **2009**, *95*, 061103.
(12) Mukherjee, A.; Prasanna, M.; Lane, M.; Go, R.; Dunayevskiy, I.; Tsekoun, A.; Patel, C. *Appl. Opt.* **2008**, *47*, 4884-4887
(13) Giglio, M.; Patimisco, P.; Sampaolo, A.; Zifarelli, A.; Blanchard, R.; Pfluegl, C.; Witinski, M.F.; Vakhshoori, D.; Tittel, F.K. *Appl. Phys. Lett.* **2018**, *113*, 171101.
(14) Sampaolo, A.; Csutak, S.; Patimisco, P.; Giglio, M.; Menduni, G.; Passaro, V.; Tittel, F.K.; Deffenbaugh, M.; Spagnolo, V. *Sens. Actuat B-Chem* **2019**, *282*, 952-960.
(15) Ma, Y.; Lewicki, R.; Razeghi, M.; Tittel, F. K. *Opt. Express* **2013**, *21.1*, 1008-1019.
(16) L. Dong, L.; Wright, J.; Peters, B.; Ferguson, B.A.; Tittel, F.K.; McWhorter, S. *Appl. Phys. B* **2012**, *107.2*, 459-467.
(17) Besson, J.P.; Schilt, S.; Thévenaz, L. *Spectrochim. Acta A Mol. Biomol. Spectrosc.* **2006**, *63.5*, 899-904.
(18) Zhang, Q.; Chang, J.; Cong, Z.; Sun, J.; Wang, Z. *IEEE Photon.* J. **2018**, *10*, 6804308.
(19) Oh, D.B.; Paige, M.E.; Bomse, D.S. *Appl. Opt.* **1998**, *37*, 2499-2501.

(20) Yu, Y.; Sanchez, N.P.; Yi, F.; Zheng, C.; Ye, W.; Wu, H.; Griffin, R.J.; Tittel, F.K. *Appl. Phys. B* **2017**, 123 164.
(21) Wysocki, G.; Bakhirkin, Y.; So, S.; Tittel, F.K.; Hill, C.J.; Yang, R.Q. *Appl. Opt.* **2007**, *46*, 8202-8210.
(22) Patimisco, P.; Sampaolo, A.; Giglio, M.; Dello Russo, S.; Mackowiak, V.; Rossmadl, H.; Cable, A.; Tittel, F. K.; Spagnolo, V. *Opt. Express* **2019**, *27*, 1401-1415.
(23) Wu, H.; Yin, X.; Dong, L.; Pei, K.; Sampaolo, A.; Patimisco, P.; Zheng, L.; Ma, W.; Zhang, L.; Yin, W.; Xiao, L.; Spagnolo, V.; Jia, S.; Tittel, F.K. *Appl. Phys. Lett.* **2017**, *110*, 121104.
(24) Tittel, F.K.; Sampaolo, A.; Patimisco, P.; Dong, L.; Geras, A.; Starecki, T.; Spagnolo, V. *Opt. Express* **2016**, *24*, A682-A692.
(25) Giglio, M.; Elefante, A.; Patimisco, P.; Sampaolo, A.; Sgobba, F.; Rossmadl, H.; Mackowiak, V.; Wu, H.; Tittel, F.K.; Dong, L.; Spagnolo, V. *Opt. Express* **2019**, *27*, 4271-4280.
(26) Patimisco, P.; Sampaolo, A.; Zheng, H.; Dong, L.; Tittel, F.K.; Spagnolo, V. *Adv. Phys.* X **2017**, *2*, 169-187.
(27) http://www.hitran.org/

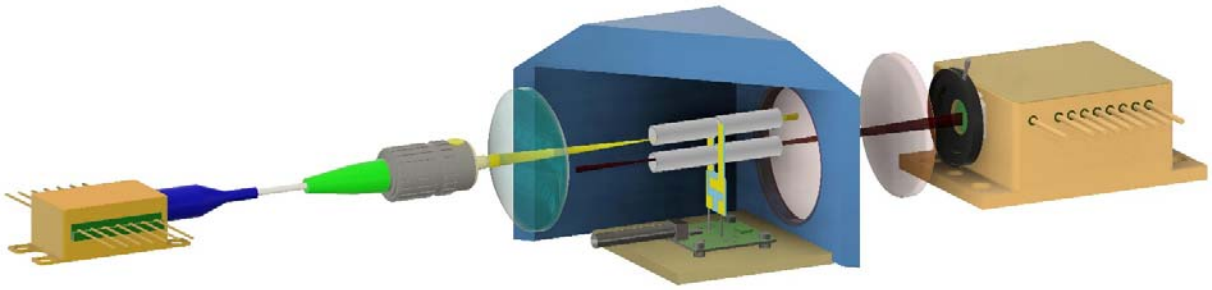

For Table of Contents Only